

NONADIABATIC MAGNETOHYDRODYNAMIC WAVES IN A CYLINDRICAL PROMINENCE THREAD WITH MASS FLOW

R. SOLER, R. OLIVER, AND J. L. BALLESTER

Departament de Física, Universitat de les Illes Balears, E-07122, Palma de Mallorca, Spain;
roberto.soler@uib.es, ramon.oliver@uib.es, joseluis.ballester@uib.es

Received 2008 March 17; accepted 2008 May 20

ABSTRACT

High-resolution observations show that oscillations and waves in prominence threads are common and that they are attenuated in a few periods. In addition, observers have also reported the presence of material flows in such prominence fine-structures. Here we investigate the time damping of nonleaky oscillations supported by a homogeneous cylindrical prominence thread embedded in an unbounded corona and with a steady mass flow. Thermal conduction and radiative losses are taken into account as damping mechanisms, and the effect of these nonideal effects and the steady flow on the attenuation of oscillations is assessed. We solve the general dispersion relation for linear, non-adiabatic magnetoacoustic and thermal waves supported by the model and find that slow and thermal modes are efficiently attenuated by nonadiabatic mechanisms. On the contrary, fast kink modes are much less affected and their damping times are much larger than those observed. The presence of flow has no effect on the damping of slow and thermal waves, whereas fast kink waves are more (less) attenuated when they propagate parallel (antiparallel) to the flow direction. Although the presence of steady mass flows improves the efficiency of nonadiabatic mechanisms on the attenuation of transverse, kink oscillations for propagation parallel to the flow, its effect is still not enough to obtain damping times compatible with observations.

Subject headings: Sun: corona — Sun: magnetic fields — Sun: oscillations — Sun: prominences

1. INTRODUCTION

Prominences and filaments are large-scale magnetic structures embedded in the solar corona and whose plasma density and temperature are akin to those of the chromosphere. High-resolution images of solar filaments (e.g., Lin et al. 2003, 2005, 2007) clearly show the existence of horizontal fine-structures within the filament body. This observational evidence suggests that prominences are composed of many field-aligned threads. These threads are usually skewed with respect to the filament long axis by an angle of 20° on average, although their orientation can vary significantly within the same prominence (Lin 2004). The observed thickness, d , and length, l , of threads are typically in the ranges $0.2'' < d < 0.6''$ and $5'' < l < 20''$ (Lin et al. 2005). Since the observed thickness is close to the resolution of present-day telescopes, it is likely that even thinner threads could exist. According to some models (e.g., Ballester & Priest 1989), a thread is believed to be part of a larger magnetic coronal flux tube which is anchored in the photosphere, with denser and cooler material near its apex, i.e., the observed thread itself. However, the process that leads to the formation of such structures is still unknown.

There is much evidence of small-amplitude waves and oscillatory motions in quiescent prominences (this topic has been reviewed by Oliver & Ballester 2002; Ballester 2006; Banerjee et al. 2007). Focusing on prominence fine-structures, some observers have detected oscillations and traveling waves in individual threads or groups of threads (Yi et al. 1991; Yi & Engvold 1991; Lin 2004; Lin et al. 2007), with periods typically between 3 and 20 minutes. In addition, mass flows along filament threads, with a flow velocity in the range $5\text{--}25\text{ km s}^{-1}$, have also been observed (Zirker et al. 1998; Lin et al. 2003, 2005). Moreover, it is noticeable that Zirker et al. (1998) and Lin et al. (2003) have detected flows in opposite directions within adjacent threads, a phenomenon known as counterstreaming. On the other hand, some observational works have suggested signatures of wave damping in prominence

oscillations (Landman et al. 1977; Tsubaki & Takeuchi 1986; Lin 2004), but to date only Molowny-Horas et al. (1999) and Terradas et al. (2002) have studied in detail this phenomenon, in particular in two-dimensional Doppler velocity time series. This analysis showed that oscillations detected in large areas of a quiescent prominence were attenuated after a few periods. Although this quick attenuation seems to be a common feature of prominence oscillations, unfortunately no similar observational study focusing on the attenuation of individual thread oscillations has been performed yet.

From the theoretical point of view, the usual interpretation of thread oscillations is in terms of the adiabatic magnetohydrodynamic eigenmodes supported by the thread body. The first investigation of individual thread vibrations was performed by Joarder et al. (1997), whose work was extended and corrected by Díaz et al. (2001), considering a nonisothermal Cartesian thread surrounded by the coronal medium (based on the model by Ballester & Priest 1989), in the $\beta = 0$ approximation. These authors found that only the low-frequency oscillatory modes are confined within the dense region, and that perturbations can achieve large amplitudes in the corona at long distances from the thread. Later, Díaz et al. (2003) assumed the same geometry, but took longitudinal propagation into account, and obtained a better confinement for the perturbations. Considering a more realistic and representative cylindrical geometry, Díaz et al. (2002) found that a nonisothermal cylindrical thread supports an even smaller number of trapped oscillations and that perturbations are much more efficiently confined within the cylinder in comparison with the Cartesian case. It is worthwhile to mention that the collective oscillations of multithread systems have also been investigated by Díaz et al. (2005) and Díaz & Roberts (2006), again in Cartesian geometry. See Ballester (2006) for a review about theoretical works.

The effect of steady mass flows on the oscillatory modes of magnetic structures has been theoretically investigated in some

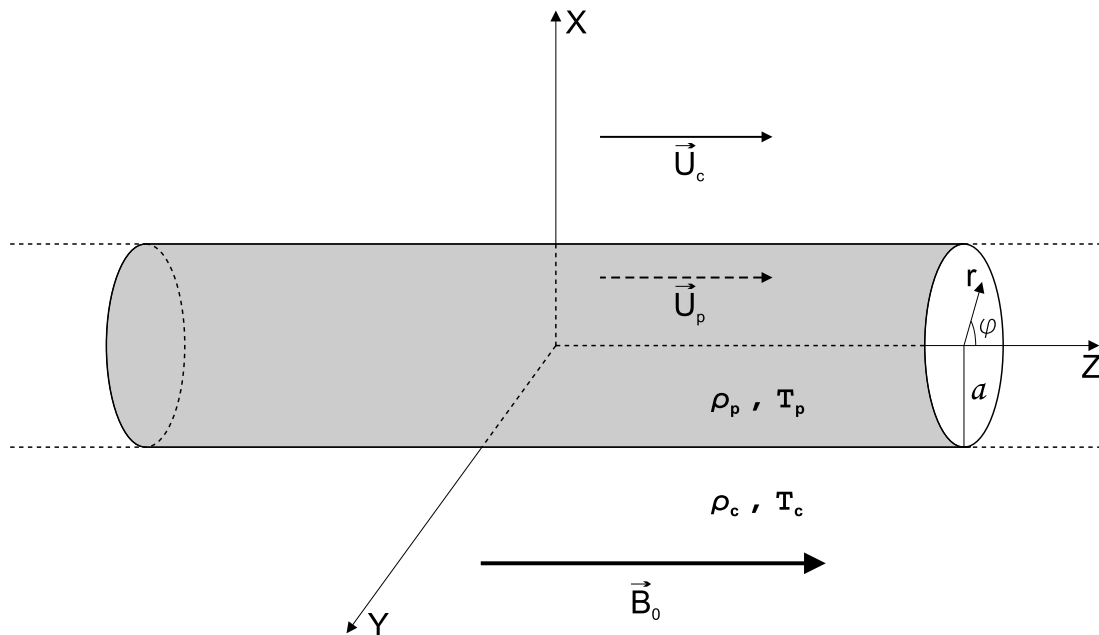


FIG. 1.— Sketch of the model.

works. The most relevant ones for the present investigation are Nakariakov & Roberts (1995), who studied the effect of steady flow in coronal and photospheric slabs, and Terra-Homem et al. (2003), who extended the former study to cylindrical geometry. In addition to producing a shift of the oscillatory frequency, both papers show that the main effect of the flow is to break the symmetry between wave propagation parallel and antiparallel to the flow direction and, for sufficiently strong flows, that slow modes can only propagate parallel to the flow direction, antiparallel propagation being forbidden.

Turning to the damping of oscillations, its theoretical investigation has been undertaken by a number of recent papers. Among the proposed damping mechanisms to explain the attenuation (Ballai 2003), nonadiabatic effects are the most extensively investigated to date, although other candidates like wave leakage (Schutgens 1997a, 1997b; Schutgens & Tóth 1999) and ion-neutral collisions (Forteza et al. 2007) have also been studied. By removing the adiabatic assumption and taking into account thermal conduction and radiative losses as damping mechanisms, some works have studied the time damping in a homogeneous, unbounded plasma (Carbonell et al. 2004), in an isolated prominence slab (Terradas et al. 2005), and in a prominence slab embedded in the solar corona (Soler et al. 2007a, hereafter Paper I; Soler et al. 2008). The common main result of these studies is that nonadiabatic mechanisms can explain the observed damping times in the case of slow modes, whereas fast modes are much less attenuated by nonadiabatic effects. It is important to note that all these articles have studied the wave attenuation in models which attempt to represent the whole prominence body. Thus, none of them have neither considered the prominence fine-structure nor mass flows.

More recently, Carbonell et al. (2008) have performed the first attempt to study the combined effect of both nonadiabatic mechanisms and steady flows on the time damping of slow and thermal waves in a homogeneous, unbounded prominence plasma. These authors found that the mass flow does not modify the damping time of both slow and thermal waves with respect to the case without flow, but the period of the slow wave increases dramati-

cally for flow velocities close to the nonadiabatic sound speed. Moreover, the thermal disturbance behaves as a propagating mode in the presence of flow. The present work goes a step forward with respect to Carbonell et al. (2008), since a more complicated geometry is assumed here. Our aim is to describe the effect of both mass flow and nonadiabatic effects on the oscillations supported by an individual prominence thread modeled as a homogeneous and infinite cylinder embedded in an unbounded and also homogeneous corona. For simplicity, the hot, coronal part of the magnetic tube that contains the thread is not taken into account. Gravity is also discarded. The inclusion of gravity would involve the consideration of a more complicated magnetic structure able to support the prominence material (e.g., Ballester & Priest 1989; Schmitt & Degenhardt 1995; Rempel et al. 1999). However, these kinds of configurations are unstable and incomplete, since they do not incorporate the physics that lead to stable solutions and, moreover, the obtained prominence widths are much smaller than those observed. Although some prominences and threads show unstable behavior, there are a number of observations of stable oscillating threads (e.g., Lin et al. 2003, 2005, 2007). For this reason and since the present work is focused on the study of waves in stable threads, we neglect the effect of gravity and consider a stable simplified model that allows us to deal with wave solutions.

This paper is organized as follows. The description of the model configuration and the basic equations for the discussion of linear nonadiabatic waves are given in § 2. Then, the results are presented in § 3, first for the case without flow and later extended by including a steady mass flow in the equilibrium. Finally, § 4 contains our conclusions.

2. MODEL EQUATIONS

The model configuration considered in the present work (Fig. 1) is made of a homogeneous and isothermal plasma cylinder of radius a with prominence conditions (density ρ_p and temperature T_p) embedded in an unbounded corona (density ρ_c and temperature T_c). The cylinder is also unlimited in the axial direction. The internal temperature and density, as well as the coronal temperature, are considered as free parameters. However, the value

of the coronal density is given by imposing total pressure continuity across the interface between the flux tube and the external medium. In all the following expressions, the subscript 0 indicates local values, while subscripts p and c denote quantities explicitly computed with prominence and coronal parameters, respectively.

Given the model geometry, we use cylindrical coordinates, namely, r , φ , and z , for the radial, azimuthal, and longitudinal coordinates, respectively. The magnetic field is uniform and orientated along the cylinder axis, $\mathbf{B}_0 = B_0 \hat{\mathbf{e}}_z$, B_0 being the same constant in the thread and in the coronal medium. A steady mass flow is assumed along the z -direction, whose flow velocity can be different in the cylinder and in the corona. Thus, $\mathbf{U}_p = U_p \hat{\mathbf{e}}_z$ and $\mathbf{U}_c = U_c \hat{\mathbf{e}}_z$ correspond to the steady flow in the flux tube and in the corona, respectively.

Parallel thermal conduction to the magnetic field, radiative losses, and heating are considered as nonadiabatic effects. We assume that the plasma is fully ionized, and so the cross field or perpendicular thermal conduction is absolutely negligible. The contribution of neutrals to the thermal conduction in a partially ionized plasma has been investigated by Forteza et al. (2008). Radiation and heating are evaluated together by means of the heat-loss function, $L(\rho, T) = \chi^* \rho T^\alpha - h \rho^a T^b$, in which radiation is parameterized with χ^* and α (Hildner 1974) and the heating scenario is given by the exponents a^* and b^* (Rosner et al. 1978; Dahlburg & Mariska 1988). Since the results for different heating scenarios do not show significant differences for prominence conditions (Carbonell et al. 2004; Terradas et al. 2005; Paper I; Soler et al. 2008), here we restrict ourselves to a constant heating per unit volume ($a^* = b^* = 0$).

The basic equations for the discussion of nonadiabatic oscillations supported by this equilibrium correspond to equations (1)–(6) of Paper I, whose linearized version applied to the present case is given as

$$\frac{\partial \rho_1}{\partial t} + U_0 \frac{\partial \rho_1}{\partial z} + \rho_0 \nabla \cdot \mathbf{v}_1 = 0, \quad (1)$$

$$\rho_0 \frac{\partial \mathbf{v}_1}{\partial t} + \rho_0 U_0 \frac{\partial \mathbf{v}_1}{\partial z} = -\nabla p_1 + \frac{1}{\mu} (\nabla \times \mathbf{B}_1) \times \mathbf{B}_0, \quad (2)$$

$$\begin{aligned} \frac{\partial p_1}{\partial t} + \rho_0 U_0 \frac{\partial p_1}{\partial z} - c_s^2 \left(\frac{\partial \rho_1}{\partial t} + \rho_0 U_0 \frac{\partial \rho_1}{\partial z} \right) \\ + (\gamma - 1) \left(\rho_0 L_\rho \rho_1 + \rho_0 L_T T_1 - \kappa_{\parallel} \frac{\partial^2 T_1}{\partial z^2} \right) = 0, \end{aligned} \quad (3)$$

$$\frac{\partial \mathbf{B}_1}{\partial t} + U_0 \frac{\partial \mathbf{B}_1}{\partial z} = \nabla \times (\mathbf{v}_1 \times \mathbf{B}_0), \quad (4)$$

$$\nabla \cdot \mathbf{B}_1 = 0, \quad (5)$$

$$\frac{p_1}{p_0} - \frac{\rho_1}{\rho_0} - \frac{T_1}{T_0} = 0. \quad (6)$$

Here, p_0 , ρ_0 , T_0 , \mathbf{B}_0 , and U_0 are the equilibrium gas pressure, density, temperature, magnetic field, and flow velocity, respectively. We also have that p_1 , ρ_1 , T_1 , $\mathbf{B}_1 = B_r \hat{\mathbf{e}}_r + B_\varphi \hat{\mathbf{e}}_\varphi + B_z \hat{\mathbf{e}}_z$, and $\mathbf{v}_1 = v_r \hat{\mathbf{e}}_r + v_\varphi \hat{\mathbf{e}}_\varphi + v_z \hat{\mathbf{e}}_z$ are the linear gas pressure, density, temperature, magnetic field, and velocity perturbations, respectively. Finally, $c_s^2 = \gamma p_0 / \rho_0$ is the adiabatic sound speed squared, $\kappa_{\parallel} = 10^{-11} T^{5/2} \text{ W m}^{-1} \text{ K}^{-1}$ is the thermal conductivity parallel to the magnetic field, and L_ρ and L_T are the partial derivatives of the heat-loss function with respect to density and temperature, respectively (see Paper I for details).

Assuming perturbations of the form $\tilde{f}_1(r, \varphi) \exp(i\omega t - ik_z z)$, where ω is the (complex) oscillatory frequency and k_z is the (real)

longitudinal wavenumber, one can combine equations (3) and (6) to obtain the following relation between the perturbed pressure and density,

$$p_1 = \tilde{\Lambda}_0^2 \rho_1, \quad (7)$$

with

$$\tilde{\Lambda}_0^2 \equiv \frac{c_s^2}{\gamma} \left[\frac{(\gamma - 1) [(T_0/p_0) \kappa_{\parallel} k_z^2 + \omega_T - \omega_\rho] + i\gamma \Omega_0}{(\gamma - 1) [(T_0/p_0) \kappa_{\parallel} k_z^2 + \omega_T] + i\Omega_0} \right], \quad (8)$$

where $\Omega_0 = \omega - U_0 k_z$ is the Doppler-shifted frequency (Terra-Homem et al. 2003), and ω_ρ and ω_T are defined in Paper I. We see that the complex quantity $\tilde{\Lambda}_0$ is a generalization, due to the presence of the flow, of the nonadiabatic sound speed defined in Paper I. The real part of $\tilde{\Lambda}_0$ plays the role of the sound speed when nonadiabatic effects are present. By means of this definition, one can see that the effect of nonadiabatic terms is to modify the medium sound speed, and so they most probably affect slow modes, since they are mainly governed by acoustic effects. See § 3.2.3 for more details about this quantity.

Now, following Terra-Homem et al. (2003), we combine the basic equations and arrive at the following expressions,

$$\Upsilon^2 [\Upsilon^2 - (\tilde{\Lambda}_0^2 + v_A^2) \nabla^2] \Delta + \tilde{\Lambda}_0^2 v_A^2 \frac{\partial^2}{\partial z^2} \nabla^2 \Delta = 0, \quad (9)$$

$$\left(\Upsilon^2 - v_A^2 \frac{\partial^2}{\partial z^2} \right) \Gamma = 0, \quad (10)$$

where $v_A^2 = B_0^2 / \mu \rho_0$ is the Alfvén speed squared, Υ is a linear operator defined as

$$\Upsilon = \frac{\partial}{\partial t} + U_0 \frac{\partial}{\partial z}, \quad (11)$$

and Δ and Γ are the divergence and the z -component of the rotational of the velocity perturbation, respectively,

$$\Delta = \nabla \cdot \mathbf{v}_1, \quad (12)$$

$$\Gamma = (\nabla \times \mathbf{v}_1) \cdot \hat{\mathbf{e}}_z. \quad (13)$$

Equation (10) is the same as equation (14) of Terra-Homem et al. (2003) and governs torsional, Alfvén waves, which are not damped by nonadiabatic mechanisms and so are not considered in the present investigation. On the other hand, equation (9) represents fast and slow magnetosonic waves, together with the thermal or condensation mode (Field 1965). If nonadiabatic terms are neglected, $\tilde{\Lambda}_0 = c_s$ and then our equation (9) reduces to equation (13) of Terra-Homem et al. (2003), which in the absence of flow ($U_0 = 0$) is equivalent to the well-known equation (17) of Lighthill (1960).

Next, the cylindrical symmetry of the model allows us to write the divergence of the velocity perturbation in the following form,

$$\Delta = R(r) \exp(i\omega t + in\varphi - ik_z z), \quad (14)$$

where n is an integer that plays the role of the azimuthal wavenumber. Expressions for the perturbed quantities as a function of Δ can be found in Appendix A. Now, applying this last expression to equation (9), one finds that $R(r)$ satisfies the well-known Bessel equation of order n ,

$$r^2 \frac{d^2 R}{dr^2} + r \frac{dR}{dr} + (m_0^2 r^2 - n^2) R = 0, \quad (15)$$

with

$$m_0^2 = \frac{(\Omega_0^2 - k_z^2 v_A^2)(\Omega_0^2 - k_z^2 \tilde{\Lambda}_0^2)}{(v_A^2 + \tilde{\Lambda}_0^2)(\Omega_0^2 - k_z^2 \tilde{c}_{T_0}^2)}, \quad (16)$$

$$\tilde{c}_{T_0}^2 \equiv \frac{v_A^2 \tilde{\Lambda}_0^2}{v_A^2 + \tilde{\Lambda}_0^2}. \quad (17)$$

The radial wavenumber squared, m_0^2 , is in general a complex quantity; hence, no pure bodylike or surfacelike waves are possible in nonadiabatic magnetoacoustics. If one assumes that $|\operatorname{Re}(m_0^2)| > |\operatorname{Im}(m_0^2)|$ (i.e., nonadiabatic effects produce a small correction to the adiabatic wave modes), the dominant wave character depends on the sign of $\operatorname{Re}(m_0^2)$. Thus, oscillations are *mainly* bodylike if $\operatorname{Re}(m_0^2) > 0$ and solutions of equation (15) are Bessel functions. On the contrary, if $\operatorname{Re}(m_0^2) < 0$, oscillations are *mainly* surfacelike (or evanescent) and solutions of equation (15) are modified Bessel functions. In this work we assume no wave propagation in the coronal medium, so the evanescent condition in the corona is imposed on the perturbations, namely, $\operatorname{Re}(m_c^2) < 0$. On the other hand, the present ordering of sound and Alfvén speeds does not permit the existence of surface waves within the fibril, so $\operatorname{Re}(m_p^2) > 0$ is assumed. Then $R(r)$ is a piecewise function,

$$R(r) = \begin{cases} A_1 J_n(m_p r), & r \leq a, \\ A_2 K_n(n_c r), & r > a, \end{cases} \quad (18)$$

with $n_c^2 = -m_c^2$, A_1 and A_2 being complex constants. The functions J_n and K_n are the usual Bessel and modified Bessel functions of order n , respectively (Abramowitz & Stegun 1972). In order to obtain the dispersion relation that governs the behavior of wave modes, we impose the continuity of the Lagrangian radial displacement, v_r/Ω_0 , and the total pressure perturbation, p_{T_1} , at the cylinder edge, $r = a$. After some algebra, the following expression is obtained,

$$\frac{\rho_c}{\rho_p} \left(\Omega_c^2 - k_z^2 v_{A,c}^2 \right) m_p \frac{J'_n(m_p a)}{J_n(m_p a)} = \left(\Omega_p^2 - k_z^2 v_{A,p}^2 \right) n_c \frac{K'_n(n_c a)}{K_n(n_c a)}, \quad (19)$$

where the prime denotes the derivative taken with respect to r . Equation (19) is formally identical to equation (21) of Terra-Homem et al. (2003), since our nonadiabatic terms are enclosed in the definition of m_p and n_c . If both nonadiabatic effects and the flow are dropped, equation (19) simply reduces to the well-known dispersion relation of Edwin & Roberts (1983).

The solution of equation (19) for a real k_z is a complex frequency, $\omega = \omega_R + i\omega_I$. The oscillatory period (P), damping time (τ_D), and the ratio of both quantities are computed as follows,

$$P = \frac{2\pi}{|\omega_R|}, \quad \tau_D = \frac{1}{\omega_I}, \quad \frac{\tau_D}{P} = \frac{1}{2\pi} \frac{|\omega_R|}{\omega_I}. \quad (20)$$

3. RESULTS

3.1. Configuration without Flow

In this section we first perform a study of the solutions of the dispersion relation (eq. [19]) in the absence of steady flow. In this case, $U_p = U_c = 0$ and so $\Omega_p = \Omega_c = \omega$. This situation corresponds to the case studied by Edwin & Roberts (1983) with the addition of nonadiabatic effects. Unless otherwise stated, the following equilibrium parameters are used in all computations: $T_p = 8000$ K,

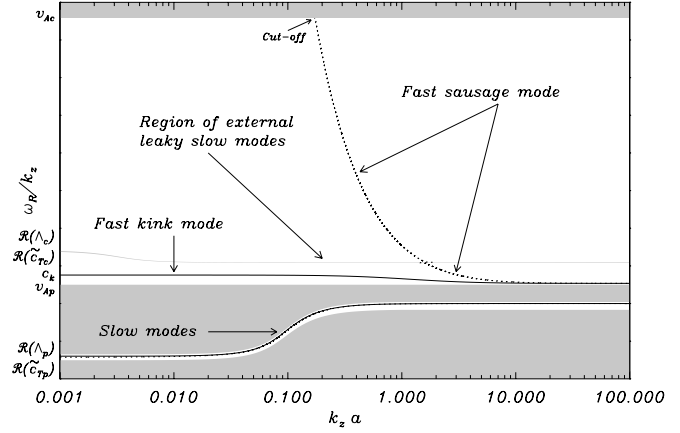


FIG. 2.—Phase speed (ω_R/k_z) vs. the dimensionless longitudinal wavenumber ($k_z a$) for the fundamental magnetoacoustic modes with $n = 1$ (solid line) and 0 (dashed line). The shaded zones are projections of the leaky regions on the plane of this diagram. Note the cutoff frequency of the fundamental fast sausage mode. The vertical axis is not drawn to scale.

$\rho_p = 5 \times 10^{-11}$ kg m $^{-3}$, $T_c = 10^6$ K, $\rho_c = 2.5 \times 10^{-13}$ kg m $^{-3}$, $B_0 = 5$ G, and $a = 30$ km. Thus, the characteristic speeds of the internal and external media are $c_{T,p} = 11.56$ km s $^{-1}$, $c_{s,p} = 11.76$ km s $^{-1}$, $v_{A,p} = 63.08$ km s $^{-1}$, $c_{T,c} = 163.51$ km s $^{-1}$, $c_{s,c} = 166.33$ km s $^{-1}$, and $v_{A,c} = 892.06$ km s $^{-1}$. In addition, both prominence and coronal plasmas are taken as optically thin (see Table 1 in Paper I for the values of parameters χ^* and α of the heat-loss function).

In the absence of flow, the complex oscillatory frequencies obtained by solving equation (19) for a fixed, real, and positive k_z appear in pairs, $\omega_1 = \omega_R + i\omega_I$ and $\omega_2 = -\omega_R + i\omega_I$. The solution ω_1 corresponds to a wave propagating toward the positive z -direction (parallel to magnetic field lines), whereas ω_2 corresponds to a wave that propagates toward the negative z -direction (antiparallel to magnetic field lines). For short, we call them parallel and antiparallel waves, respectively. Both parallel and antiparallel wave modes are equivalent and show exactly the same physical properties when no flow is considered. For the sake of simplicity, the results presented in this section correspond to parallel waves, which have a positive phase speed. Equivalent results for antiparallel waves are deduced by considering negative phase speeds.

3.1.1. Dispersion Diagram and Eigenfunctions of Magnetoacoustic Modes

Magnetoacoustic modes supported by a magnetic cylinder have been extensively investigated (e.g., Spruit 1982; Edwin & Roberts 1983; Cally 1986). Fast oscillations with $n = 0$, $n = 1$, and $n \geq 2$ correspond to sausage, kink, and fluting or ballooning modes, respectively. On the basis that thread oscillations are observed in Doppler time series, this work is mainly focused on kink modes, which produce displacements of the thread axis from its original position. The fundamental fast kink mode is trapped for realistic values of the thickness and width of threads. Regarding slow modes, the fundamental modes and their harmonics are all trapped for any value of k_z and n , but all of them have an almost identical frequency, as in the slab case (Paper I). Thus, we also restrict ourselves to the fundamental slow mode with $n = 1$ for simplicity. An additional solution of equation (19) is the thermal mode which, in the absence of flow, has a purely imaginary frequency (see § 3.1.3).

Figure 2 displays the phase speed diagram corresponding to the fundamental modes with $n = 0$ and 1 (compare this with Fig. 2

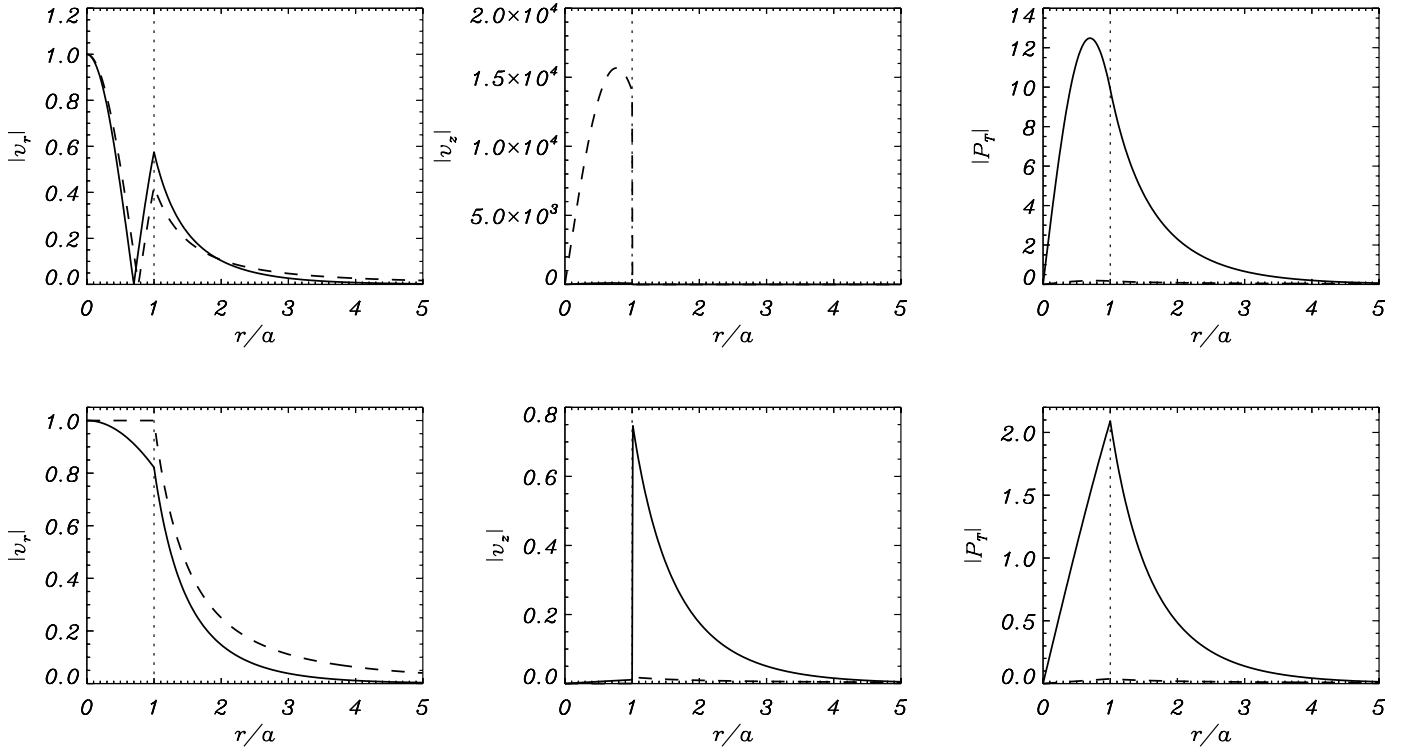


FIG. 3.—Modulus of the eigenfunctions (in arbitrary units) corresponding to the radial velocity perturbation, v_r , the longitudinal velocity perturbation, v_z , and the total pressure perturbation, P_{T1} , as functions of the dimensionless distance to the cylinder axis for the fundamental slow (*top*) and fast kink (*bottom*) modes. The solid lines correspond to $k_z a = 1$, while the dashed lines correspond to $k_z a = 10^{-2}$. Note that v_z is not continuous at the cylinder edge, whose location is denoted by the vertical dotted lines.

of Paper I). One can see that the behavior of slow modes and the fast sausage mode is similar to that in a slab. An important difference with the results of Paper I is that in the cylindrical case the fast kink mode does not couple with the external leaky slow modes enclosed in the region $\text{Re}(\tilde{c}_{Tc}) < \omega_R/k_z < \text{Re}(\tilde{\Lambda}_c)$, because its phase speed in the long-wavelength limit is $c_k < \text{Re}(\tilde{c}_{Tc})$, with $c_k^2 = (\rho_p v_{A,p}^2 + \rho_c v_{A,c}^2)/(\rho_p + \rho_c)$.

Next, we plot in Figure 3 the eigenfunctions corresponding to the radial and longitudinal velocity perturbations, v_r and v_z , and the total pressure perturbation, P_{T1} , for the fundamental slow and fast kink magnetoacoustic modes. Contrary to the slab case of Soler et al. (2007b, Fig. 4), perturbations are efficiently confined within the cylinder for any value of the longitudinal wavenumber. Thus, this suggests that the influence of the corona on the damping of oscillations could be of smaller importance than in a magnetic slab. On the other hand, the expected velocity polarization is obtained, the slow mode being mainly polarized along the longitudinal direction ($v_z \gg v_r$) and the fast kink mode being responsible for transverse, radial motions ($v_r \gg v_z$).

3.1.2. Damping Times of Fast Kink and Slow Waves and Comparison with a Longitudinal Slab

We now compute the period, damping time, and their ratio for the fundamental fast kink and slow modes for a wide range of k_z ($10^{-10} \text{ m}^{-1} < k_z < 10^{-2} \text{ m}^{-1}$). This range includes the values corresponding to the observed wavelengths in prominences ($10^{-8} \text{ m}^{-1} \lesssim k_z \lesssim 10^{-6} \text{ m}^{-1}$). In Figure 4 these results are compared with those obtained for a longitudinal slab whose half-width is equal to the cylinder radius (i.e., the case analyzed in § 4.4 of Paper I). We see that the results of the slow mode are almost identical in both cylindrical and slab geometries; hence, the reader is referred to Paper I for a description of the slow mode behavior.

On the contrary, the results of the fast kink mode show significant differences between the slab and the cylinder. For small and intermediate k_z , both the period and damping time in a cylinder are larger than in a slab. This effect is specially noticeable for the damping time in the observed range of wavelengths, since its value in the cylindrical case is more than 3 orders of magnitude larger than in the slab. This causes the ratio τ_D/P to be in the range $10^5 \lesssim \tau_D/P \lesssim 10^9$ for the observed wavelengths. Therefore, nonadiabatic effects are much less efficient in damping the fast kink mode in a cylinder than in the slab geometry. In addition, we see that the fast kink mode damping time due to nonadiabatic effects is much larger than typical lifetimes of filament threads and prominences. Hence, nonadiabatic fast kink waves are in practice undamped when these results are applied in the solar context.

3.1.3. Thermal Mode

Now we turn our attention to the thermal or condensation mode. The condensation instability has been studied in uniform, unbounded plasmas (Field 1965), in coronal slabs (van der Linden & Goossens 1991), and in coronal cylinders (An 1984). Since the thermal mode has a purely imaginary frequency, we now assume $\omega = is$, where s is real and often called the damping (or growing) rate. The situation $s > 0$ corresponds to a damped thermal mode, whereas $s < 0$ occurs if the mode is thermally unstable. The sign of s can be estimated a priori by considering the stability criterion provided by Field (1965),

$$\kappa_{\parallel,p} k_z^2 + \rho_p \left(L_{T,p} - \frac{\rho_p}{T_p} L_{\rho,p} \right) > 0. \quad (21)$$

Since for prominence conditions this inequality is verified for any real value of k_z , the thermal mode is always a damped solution,

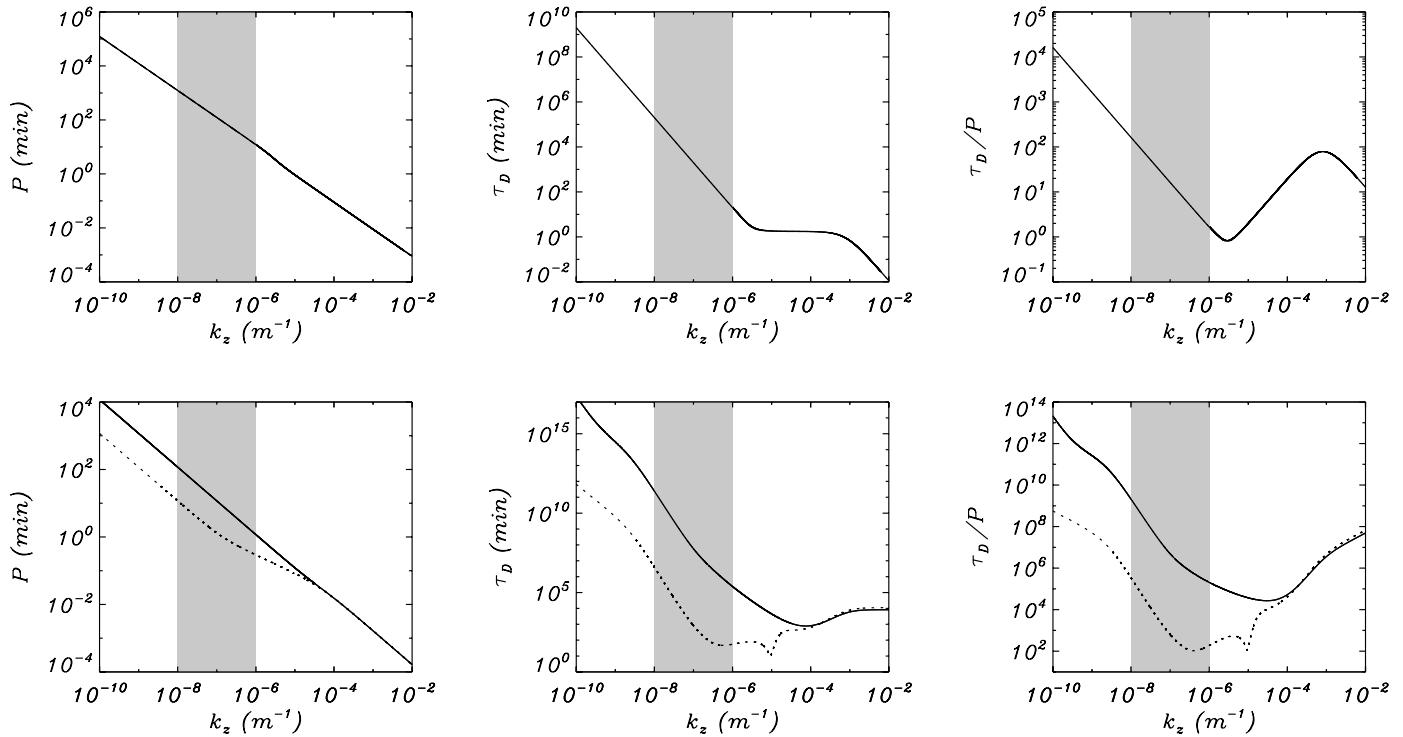


FIG. 4.—Period (left), damping time (middle), and ratio of the damping time to the period (right) vs. the longitudinal wavenumber for the fundamental oscillatory modes in the absence of flow. Top and bottom panels correspond to the slow and fast kink modes, respectively. Solid lines are the solutions of the present, cylindrical equilibrium, whereas dotted lines are the results of a longitudinal slab (Paper I). Both lines overlap in the top panels. Shaded zones indicate the range of observed wavelengths.

and therefore, we expect $s > 0$. According to van der Linden & Goossens (1991), see Appendix B for more details, the evanescent assumption in the corona ($m_c^2 < 0$) together with the body-wave assumption within the fibril ($m_p^2 > 0$) is satisfied in a narrow range of s . However, there is an extremely narrow range of k_z ($1.68 \times 10^{-7} \text{ m}^{-1} \lesssim k_z \lesssim 1.70 \times 10^{-7} \text{ m}^{-1}$) in which $m_p^2 > 0$ and $m_c^2 > 0$, and so the evanescent assumption is not verified. Then, the thermal mode does not exist as a nonleaky solution in such a range of k_z . Despite this, the fundamental thermal mode and all its harmonics have an almost identical damping rate s , whose value is also almost independent of the azimuthal wavenumber, n . For this reason and for the sake of simplicity, we again restrict ourselves to solutions with $n = 1$ and focus on the fundamental mode.

Figure 5 displays the spatial distribution of perturbations v_r , v_z , and P_{T1} corresponding to the fundamental thermal mode with $n = 1$. We see that the velocity field is dramatically polarized along the cylinder axis and that the eigenfunctions are very similar to those obtained for the slow mode (compare with Fig. 3,

top). On the other hand, the damping time ($\tau_D = 1/s$) is plotted in Figure 6 as a function of k_z . One can see that this mode is very quickly attenuated and that radiative losses from the prominence plasma are responsible for the attenuation in the observed wavelength range, whereas prominence thermal conduction is only relevant for large k_z . Coronal mechanisms have a negligible effect.

3.2. Effect of Steady Flow

Hereafter, we include a steady mass flow in the model in order to assess its influence on the oscillatory modes described above. With no loss of generality, we assume no flow in the external medium, i.e., $U_c = 0$. Moreover, the internal flow is assumed flowing toward the positive z -direction, i.e., $U_p > 0$. Note that any other possible configuration can be obtained by means of a suitable election of the reference frame.

3.2.1. Phase Speed Shift

The reader is referred to Terra-Homem et al. (2003) for a detailed description of the modification of the phase speed diagram

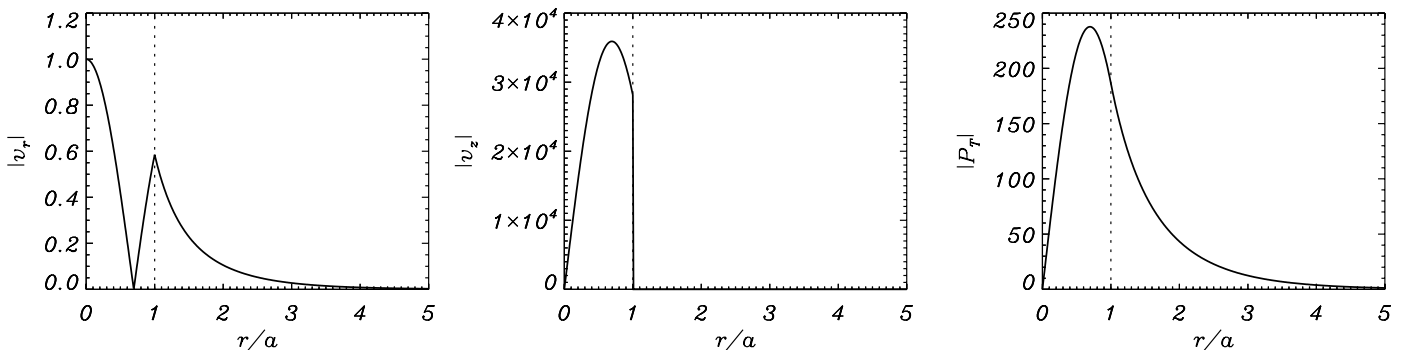


FIG. 5.—Same as Fig. 3, but for the fundamental thermal mode with $k_z a = 1$.

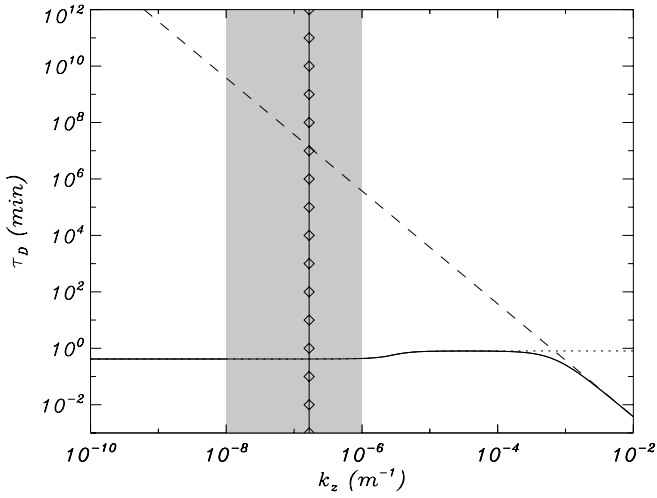


FIG. 6.—Damping time vs. the longitudinal wavenumber for the fundamental thermal mode. Different line styles represent the omitted nonadiabatic mechanism: all mechanisms considered (solid line), prominence conduction eliminated (dotted line), prominence radiation eliminated (dashed line), coronal conduction eliminated (dot-dashed line), and coronal radiation eliminated (triple-dot-dashed line). The vertical line with symbols inside the shaded zone indicates the range of k_z in which the thermal mode does not exist as a nonleaky solution (see Appendix B for details).

due to the presence of flow. In short, the symmetry between parallel ($\omega_R > 0$) and antiparallel ($\omega_R < 0$) waves is broken by the flow. Phase speeds of slow and fast parallel waves are now in the ranges $[\text{Re}(\tilde{c}_{T_p}) + U_p, \text{Re}(\tilde{\Lambda}_p) + U_p]$ and $[v_{A,p} + U_p, v_{A,c}]$, respectively. On the other hand, phase speeds of slow and fast antiparallel waves lie now within the regions $[-\text{Re}(\tilde{\Lambda}_p) + U_p, -\text{Re}(\tilde{c}_{T_p}) + U_p]$ and $[-v_{A,c}, -v_{A,p} + U_p]$, respectively. For a flow velocity larger than the internal nonadiabatic sound speed (see Carbonell et al. 2008), the phase speed of antiparallel slow waves is dragged to positive values, and so they become parallel waves in practice. These solutions were called backward waves by Nakariakov & Roberts (1995). An equivalent phenomenon can also occur for fast waves for a super-Alfvénic flow, i.e., $U_p > v_{A,p}$. Note that super-Alfvénic flows seem to be unrealistic in light of observations.

Regarding thermal modes, the real part of their frequency now acquires a positive value, and their phase speed is equal to the flow velocity. Thus, thermal modes behave as parallel-propagating waves with respect to the static, external reference frame. Although this result could be relevant for the observational point of view, since thermal modes might be detected as propagating waves in filament threads (Lin et al. 2007), their extremely quick attenuation makes them undetectable in practice.

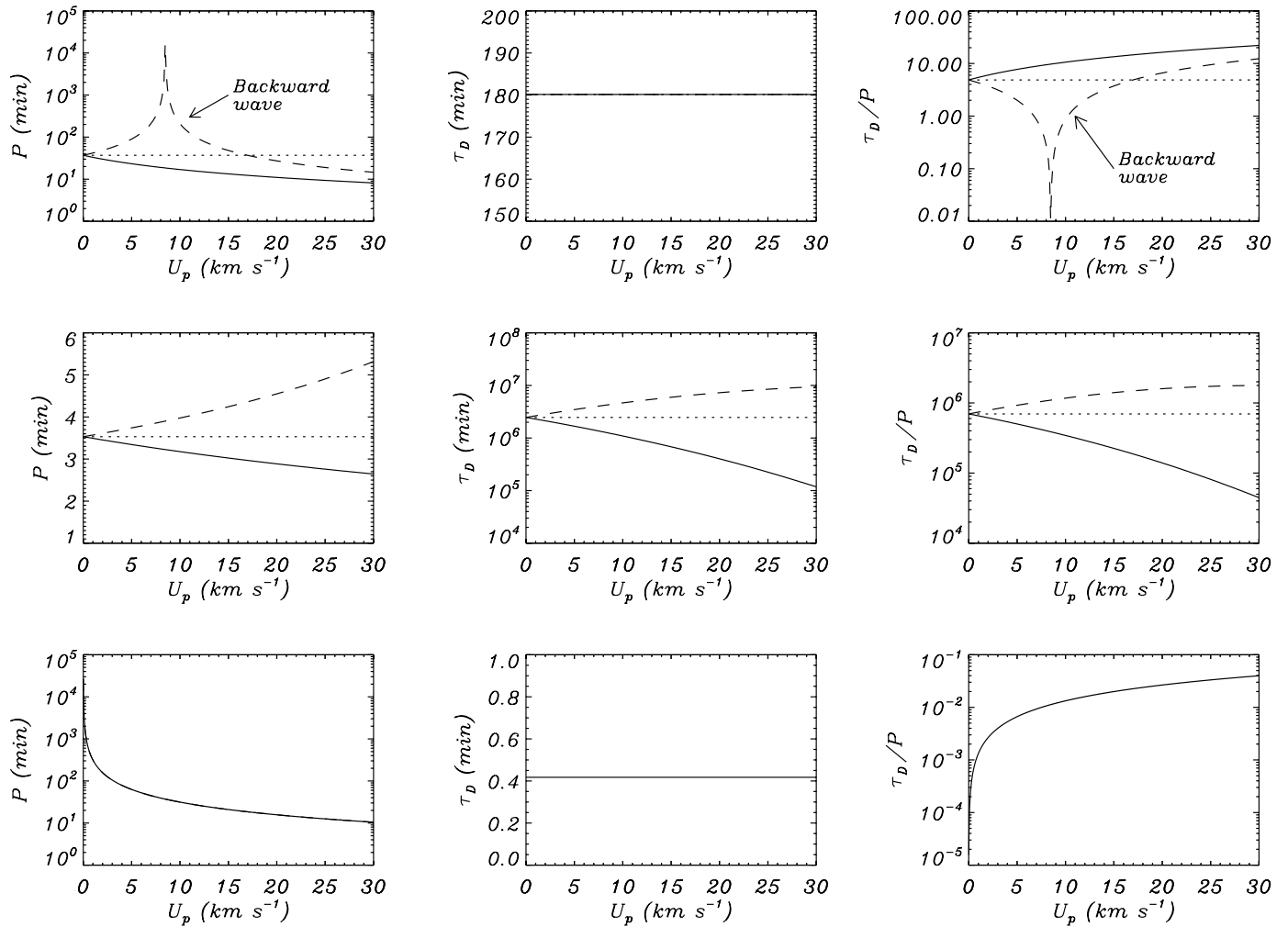


FIG. 7.—Period (left), damping time (middle), and ratio of the damping time to the period (right) vs. the flow velocity for the fundamental oscillatory modes with $k_z a = 10^{-2}$. Top, middle, and bottom panels correspond to the slow, fast kink, and thermal modes, respectively. Different line styles represent parallel waves (solid lines), antiparallel waves (dashed lines), and solutions in the absence of flow (dotted lines).

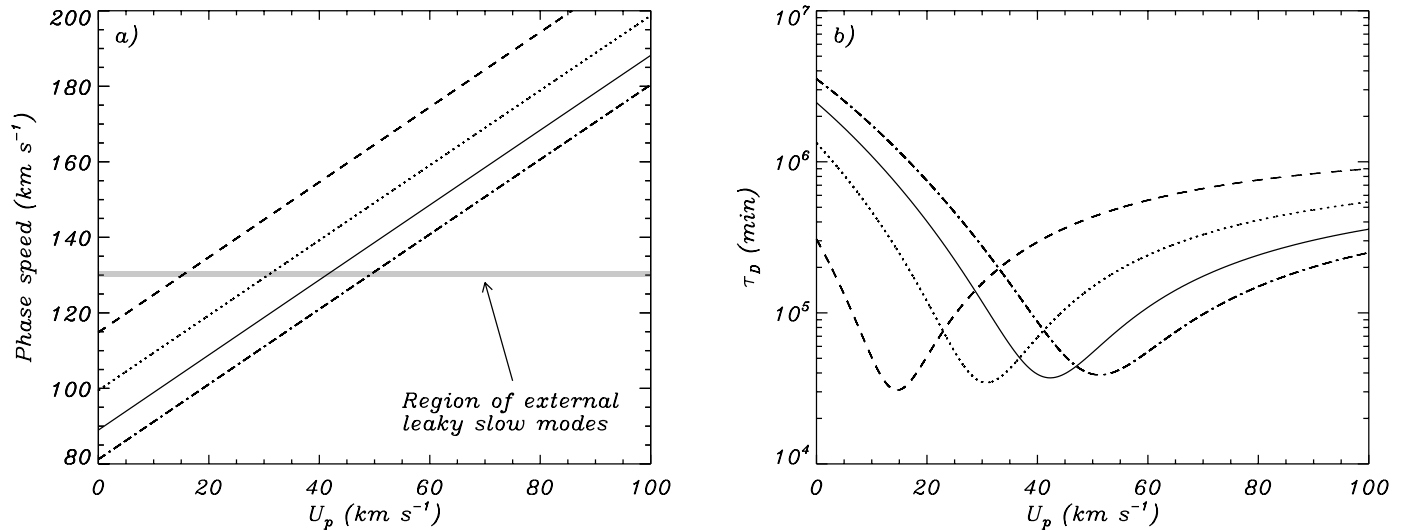


FIG. 8.—(a) Phase speed and (b) damping time vs. the flow velocity for the parallel fast kink mode with $k_z a = 10^{-2}$. Different line styles represent different values of the prominence density, $\rho_p = 5 \times 10^{-11}$ (solid lines), 4×10^{-11} (dotted lines), 3×10^{-11} (dashed lines), and 6×10^{-11} kg m^{-3} (dot-dashed lines). The shaded zone in (a) shows the region of phase speeds corresponding to external leaky slow modes.

3.2.2. Influence on the Damping Time

Regarding the effect of the flow on the damping time of oscillations, we plot in Figure 7 the dependence of the period, damping time, and their ratio as a function of the flow velocity. The longitudinal wavenumber has been fixed to $k_z a = 10^{-2}$, which corresponds to a value within the observed range of wavelengths. The flow velocity is considered in the range $0 \text{ km s}^{-1} < U_p < 30 \text{ km s}^{-1}$, which corresponds to the observed flow speeds in quiescent prominences. In agreement with Carbonell et al. (2008), the antiparallel slow wave becomes a backward wave for $U_p \approx 8.5 \text{ km s}^{-1}$, which corresponds to the nonadiabatic sound speed (eq. [8]). This causes the period of this solution to grow dramatically near this flow velocity. However, the period of both parallel and antiparallel fast kink waves is only slightly modified with respect to the solution in the absence of flow, and the thermal wave

now has a finite period, which is comparable to that of the parallel slow mode.

On the other hand, we see that the damping time of both slow and thermal modes is not affected by the presence of flow, as in Carbonell et al. (2008). Nevertheless, the attenuation of the fast kink mode in the present case is influenced by the flow. The larger the flow velocity, the more attenuated the parallel fast kink wave, whereas the opposite occurs for the antiparallel solution. This behavior can be understood with the help of Figure 8, which displays the phase speed of the parallel fast kink mode and its damping time for a wider range of the flow velocity and for different values of the thread density. We see that for a specific value of the flow velocity the parallel fast mode phase speed coincides with that of the external leaky slow modes, which is in the range $[\text{Re}(\tilde{c}_{T,c}), \text{Re}(\tilde{\Lambda}_c)]$. Then, for this flow velocity, the parallel fast kink wave couples with the external slow modes by means of a

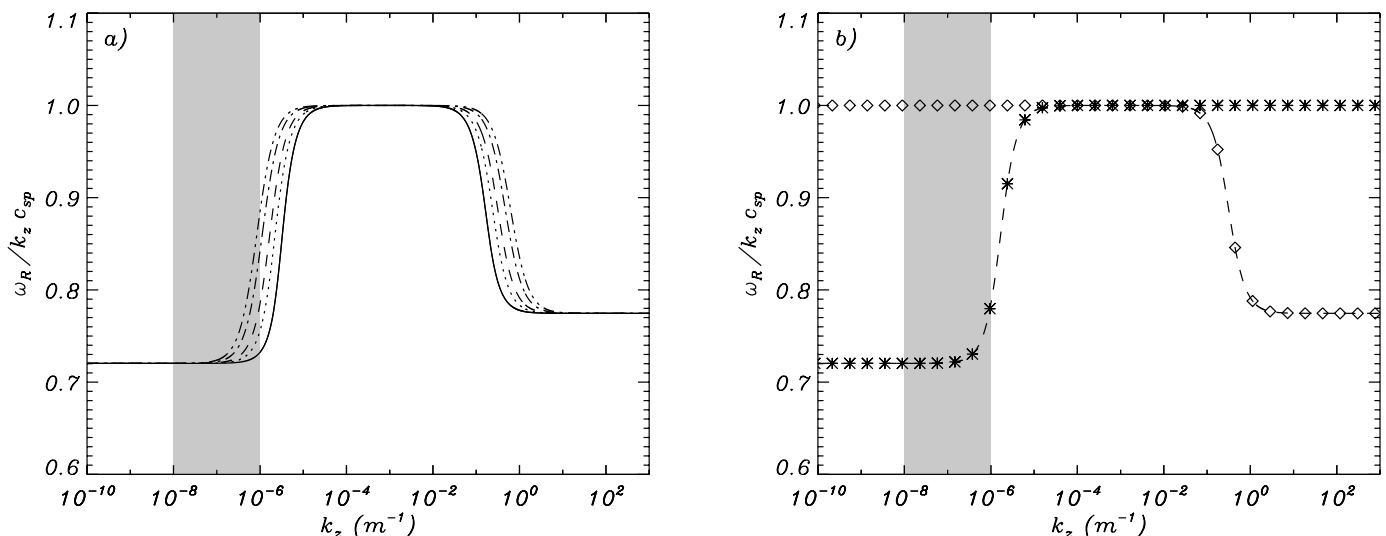


FIG. 9.—Internal nonadiabatic sound speed (in units of the internal adiabatic sound speed) vs. the longitudinal wavenumber. (a) Results for different flow velocities, $U_p = 0$ (solid line), 5 (dotted line), 10 (dashed line), 20 (dot-dashed line), and 30 km s^{-1} (dot-dot-dashed line). (b) Result for $U_p = 10 \text{ km s}^{-1}$ considering all non-adiabatic mechanisms (dashed line), neglecting prominence conduction (asterisks), and neglecting prominence radiation (diamonds). The shaded zones in both panels indicate the range of observed wavelengths.

“weak” coupling, according to the nomenclature from Soler et al. (2008). This coupling causes a minimum in the damping time as is clearly seen in Figure 8*b*. On the other hand, a similar argument can be adopted to explain the increase of the antiparallel fast mode damping time with U_p , since the phase speed of the antiparallel wave moves away to the phase speed region of (antiparallel) external slow modes, i.e., $[-\text{Re}(\tilde{\Lambda}_c), -\text{Re}(\tilde{c}_{T,c})]$, as the flow speed increases. For parallel waves, the flow velocity for which the coupling takes place depends on the thread density in such a way that the smaller the density, the smaller the flow velocity. Hence, the minimum of the damping time moves to smaller values of the flow velocity for a small thread density. Nevertheless, this minimum takes place at a flow velocity of about 40 km s^{-1} for a representative thread density of $\rho_p = 5 \times 10^{-11} \text{ km s}^{-1}$, which is a larger velocity than those observed by at least a factor of 2. Moreover, even the smallest damping time is several orders of magnitude larger than the lifetimes of prominence threads, meaning that the effect of the flow is not enough to obtain a reasonable and realistic attenuation for kink modes.

3.2.3. Nonadiabatic Sound Speed

Next, we study the influence of the steady mass flow on the value of the internal nonadiabatic sound speed. Since the internal nonadiabatic sound speed corresponds to the value of the flow velocity for which antiparallel slow waves become backward waves, it is interesting to assess its behavior of as a function of the wave-number and the flow velocity. We perform a study similar to that by Carbonell et al. (2008) and compute the internal nonadiabatic sound speed as a function of k_z for different values of the flow velocity (Fig. 9). The dependence on k_z is the one explained by Carbonell et al. (2008) and presents three different plateaus. For large k_z the dominant mechanism is prominence thermal conduction, and the nonadiabatic sound speed coincides with the isothermal value. For intermediate k_z the nonadiabatic sound speed does not depend on nonideal effects, and its value corresponds to the adiabatic sound speed. For small k_z , including the observed region of wavelengths, the nonadiabatic sound speed becomes slightly smaller than the isothermal one, and prominence radiation is the governing mechanism. On the other hand, one can see that the effect of the flow is to widen the range of k_z in which the nonadiabatic sound speed matches the adiabatic value: the larger the flow, the wider the range. For large flow velocities, the transition between the intermediate- k_z (adiabatic) and the small- k_z plateaus takes place within the observed wavelength region.

4. CONCLUSIONS

In the present work we have studied the combined effect of both nonadiabatic effects and a steady mass flow on the damping of oscillations supported by an individual, cylindrical, and homogeneous prominence thread. Our main conclusions are summarized as follows.

1. In the absence of flow, slow modes are efficiently damped by nonadiabatic effects, while fast kink waves are in practice non-attenuated, since their damping times are much larger than typical lifetimes of filament threads.

2. The damping by nonadiabatic mechanisms of transverse, kink oscillations is much less efficient in the present, cylindrical case than in the slab geometry.

3. The thermal wave is a nonpropagating solution in the absence of flow, and its attenuation by radiative losses is extremely quick.

4. The presence of flow breaks the symmetry between waves propagating parallel or antiparallel to the flow. For a flow velocity larger than the internal nonadiabatic sound speed, antiparallel slow waves become backward waves.

5. In the presence of flow, the thermal mode behaves as a wave that propagates parallel to the flow, and its motions are mainly polarized along the longitudinal direction. Nevertheless, this oscillatory behavior cannot be likely observed in practice due to its quick damping.

6. The damping time of both slow and thermal waves is not affected by the flow. On the contrary, for realistic values of the flow velocity, the larger the flow, the larger the attenuation of parallel fast kink waves, whereas the contrary occurs for antiparallel fast kink solutions. Nevertheless, this effect is not enough to obtain realistic damping times in the case of fast kink modes.

In agreement with previous studies, the consideration of non-adiabatic mechanisms provides damping times that are compatible with observations in the case of slow modes, which can be related to long-period oscillations. The main effect of the flow on these solutions is that only propagation parallel to the flow is allowed for strong enough flows. The negligible attenuation of fast kink modes in the absence of flow is slightly improved in the case of parallel waves when flow is present, the damping time being diminished by an order of magnitude for realistic flow velocities. However, the damping time is still several orders of magnitude larger than the lifetimes of filament threads, and therefore, neither nonadiabatic mechanisms nor mass flows provide reasonable fast mode damping times applicable to prominences. For this reason, it is likely that another damping mechanism is responsible for a more efficient attenuation of transverse thread motions, resonant absorption being a good candidate which should be investigated. On the other hand, the investigation of the effect of flow, and in particular counterstreaming flows, on the damping of collective transverse oscillations of cylindrical multithread models is interesting in light of the present results and could be the subject of future research.

The authors acknowledge the financial support received from the Spanish Ministerio de Ciencia y Tecnología and the Conselleria d’Economia, Hisenda i Innovació under grants AYA 2006-07637 and PCTIB 2005GC3-03, respectively. R. Soler thanks the Conselleria d’Economia, Hisenda i Innovació for a fellowship. The authors also acknowledge the International Space Science Institute for their financial support of the meetings “Coronal Waves and Oscillations” and “Spectroscopy and Imaging of Quiescent and Eruptive Solar Prominences from Space” in Bern, Switzerland, where some of the ideas relevant to this work were discussed.

APPENDIX A

EXPRESSIONS FOR THE PERTURBATIONS

Expressions for the perturbations as functions of the divergence of the perturbed velocity, $\Delta = \nabla \cdot v_1$, and its derivative are given as

$$v_r = -\frac{(\Omega_0^2 - k_z^2 \tilde{\Lambda}_0^2)}{\Omega_0^2 m_0^2} \frac{\partial \Delta}{\partial r}, \quad (\text{A1})$$

$$v_\varphi = -i \frac{(\Omega_0^2 - k_z^2 \tilde{\Lambda}_0^2) n}{\Omega_0^2 m_0^2} \frac{\Delta}{r}, \quad (\text{A2})$$

$$v_z = -i \frac{\tilde{\Lambda}_0^2 k_z}{\Omega_0^2} \Delta, \quad (\text{A3})$$

$$\rho_1 = i \frac{\rho_0}{\Omega_0} \Delta, \quad (\text{A4})$$

$$p_1 = i \frac{\rho_0 \tilde{\Lambda}_0^2}{\Omega_0} \Delta, \quad (\text{A5})$$

$$T_1 = i \frac{T_0}{\Omega_0} \left(\gamma \frac{\tilde{\Lambda}_0^2}{c_s^2} - 1 \right) \Delta, \quad (\text{A6})$$

$$B_r = -B_0 k_z \frac{(\Omega_0^2 - k_z^2 \tilde{\Lambda}_0^2)}{\Omega_0^3 m_0^2} \frac{\partial \Delta}{\partial r}, \quad (\text{A7})$$

$$B_\varphi = -i B_0 k_z \frac{(\Omega_0^2 - k_z^2 \tilde{\Lambda}_0^2) n}{\Omega_0^3 m_0^2} \frac{\Delta}{r}, \quad (\text{A8})$$

$$B_z = i B_0 \frac{(\Omega_0^2 - k_z^2 \tilde{\Lambda}_0^2)}{\Omega_0^3} \Delta, \quad (\text{A9})$$

$$p_{m_1} = i \rho_0 v_A^2 \frac{(\Omega_0^2 - k_z^2 \tilde{\Lambda}_0^2)}{\Omega_0^3} \Delta, \quad (\text{A10})$$

$$p_{T_1} = p_1 + p_{m_1} = i \rho_0 \frac{(\Omega_0^2 - k_z^2 \tilde{\Lambda}_0^2)(\Omega_0^2 - k_z^2 v_A^2)}{\Omega_0^3 m_0^2} \Delta. \quad (\text{A11})$$

APPENDIX B

REGION OF NONEXISTENCE OF THE THERMAL MODE

Following a similar argument to that used by van der Linden & Goossens (1991), let us consider that the thermal mode frequency in the absence of flow is given by $\omega = is$, with s a real quantity. So, from equation (16) one obtains

$$m_0^2 = - \frac{(s^2 + k_z^2 v_A^2)(s^2 + k_z^2 \tilde{\Lambda}_0^2)}{(v_A^2 + \tilde{\Lambda}_0^2)(s^2 + k_z^2 \tilde{c}_{T_0}^2)} = - (s^2 + k_z^2 v_A^2) \frac{\mathcal{A}}{\mathcal{B}}. \quad (\text{B1})$$

Quantities \mathcal{A} and \mathcal{B} are the following third-order polynomials in s ,

$$\mathcal{A} = s^3 - \mathcal{N}_2 s^2 + k_z^2 c_s^2 s - k_z^2 c_s^2 \mathcal{N}_2, \quad (\text{B2})$$

$$\mathcal{B} = s^3 - \mathcal{N}_3 s^2 + k_z^2 c_T^2 s - k_z^2 c_T^2 \mathcal{N}_1, \quad (\text{B3})$$

with

$$\mathcal{N}_1 = \frac{(\gamma - 1)}{\gamma} \left(\frac{T_0}{p_0} \kappa_{\parallel} k_z^2 + \omega_T - \omega_\rho \right), \quad (\text{B4})$$

$$\mathcal{N}_2 = (\gamma - 1) \left(\frac{T_0}{p_0} \kappa_{\parallel} k_z^2 + \omega_T \right), \quad (\text{B5})$$

$$\mathcal{N}_3 = \frac{\mathcal{N}_2 v_A^2 + \mathcal{N}_1 c_s^2}{v_A^2 + c_s^2}. \quad (\text{B6})$$

The condition $m_p^2 > 0$ implies that $\text{sgn}(\mathcal{A}_p) \neq \text{sgn}(\mathcal{B}_p)$. The solutions of $\mathcal{A} = 0$ are a pair of complex conjugate roots and a real root, while the same stands for the roots of $\mathcal{B} = 0$. Then, the condition $m_p^2 > 0$ is only verified in the region between the real roots of $\mathcal{A}_p = 0$ and $\mathcal{B}_p = 0$, namely, $s_{\mathcal{A}_p}$ and $s_{\mathcal{B}_p}$, respectively, which are very close to each other. On the other hand, the external evanescent requirement ($m_c^2 < 0$) is verified outside the region between the real solutions of $\mathcal{A}_c = 0$ and $\mathcal{B}_c = 0$, namely, $s_{\mathcal{A}_c}$ and $s_{\mathcal{B}_c}$, respectively. By computing these real roots (Fig. 10), one obtains that both regions do not overlap except for $5.04 \times 10^{-3} \lesssim k_z a \lesssim 5.10 \times 10^{-3}$. Thus, outside this extremely narrow overlapping region, the thermal mode exists with a damping rate in the range $s_{\mathcal{B}_p} < s < s_{\mathcal{A}_p}$, where both conditions $m_p^2 > 0$ and $m_c^2 < 0$ are satisfied.

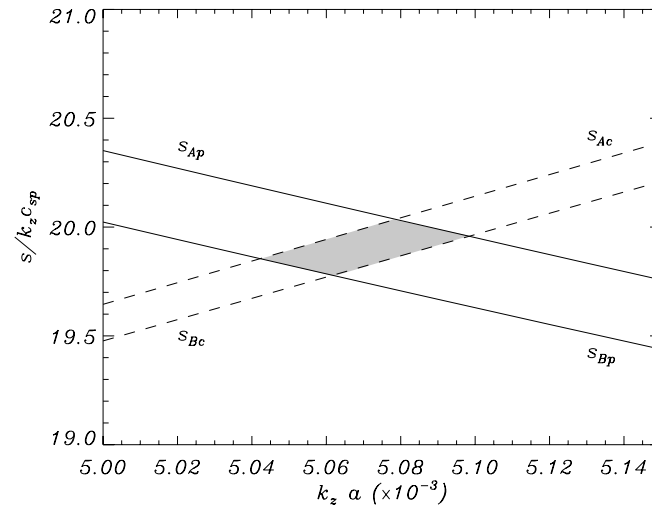


FIG. 10.—Damping rate per wavenumber vs. the wavenumber, both in dimensionless units. The shaded zone indicates the region where the thermal mode does not exist as an evanescent-like solution, i.e., the overlap of the regions where $m_p^2 > 0$ (between solid lines) and $m_c^2 > 0$ (between dashed lines) are both satisfied.

REFERENCES

- Abramowitz, M., & Stegun, I. A. 1972, *Handbook of Mathematical Functions* (New York: Dover)
- An, C.-H. 1984, *ApJ*, 276, 755
- Ballai, I. 2003, *A&A*, 410, L17
- Ballester, J. L. 2006, *Philos. Trans. R. Soc. London A*, 364, 405
- Ballester, J. L., & Priest, E. R. 1989, *A&A*, 225, 213
- Banerjee, D., Erdélyi, R., Oliver, R., & O'Shea, E. 2007, *Sol. Phys.*, 246, 3
- Cally, P. S. 1986, *Sol. Phys.*, 103, 277
- Carbonell, M., Oliver, R., & Ballester, J. L. 2004, *A&A*, 415, 739
- . 2008, *A&A*, submitted
- Dahlburg, R. B., & Mariska, J. T. 1988, *Sol. Phys.*, 117, 51
- Díaz, A. J., Oliver, R., & Ballester, J. L. 2002, *ApJ*, 580, 550
- . 2003, *A&A*, 402, 781
- . 2005, *A&A*, 440, 1167
- Díaz, A. J., Oliver, R., Erdélyi, R., & Ballester, J. L. 2001, *A&A*, 379, 1083
- Díaz, A. J., & Roberts, B. 2006, *Sol. Phys.*, 236, 111
- Edwin, P. M., & Roberts, B. 1983, *Sol. Phys.*, 88, 179
- Field, G. B. 1965, *ApJ*, 142, 531
- Forteza, P., Oliver, R., & Ballester, J. L. 2008, *A&A*, in press
- Forteza, P., Oliver, R., Ballester, J. L., & Khodachenko, M. L. 2007, *A&A*, 461, 731
- Hildner, E. 1974, *Sol. Phys.*, 35, 123
- Joarder, P. S., Nakariakov, V. M., & Roberts, B. 1997, *Sol. Phys.*, 173, 81
- Landman, D. A., Edberg, S. J., & Laney, C. D. 1977, *ApJ*, 218, 888
- Lighthill, M. J. 1960, *Philos. Trans. R. Soc. London A*, 252, 397
- Lin, Y. 2004, Ph.D. thesis, Univ. Oslo
- Lin, Y., Engvold, O., Rouppe van der Voort, L. H. M., & van Noort, M. 2007, *Sol. Phys.*, 246, 65
- Lin, Y., Engvold, O., Rouppe van der Voort, L. H. M., Wiik, J. E., & Berger, T. E. 2005, *Sol. Phys.*, 226, 239
- Lin, Y., Engvold, O., & Wiik, J. E. 2003, *Sol. Phys.*, 216, 109
- Molowny-Horas, R., Wiehr, E., Balthasar, H., Oliver, R., & Ballester, J. L. 1999, in *JOSO Ann. Rep. 1998*, ed. A. Antalová, H. Balthasar, & A. Kucera, 126
- Nakariakov, V. M., & Roberts, B. 1995, *Sol. Phys.*, 159, 213
- Oliver, R., & Ballester, J. L. 2002, *Sol. Phys.*, 206, 45
- Rempel, M., Schmitt, D., & Glatzel, W. 1999, *A&A*, 343, 615
- Rosner, R., Tucker, W. H., & Vaiana, G. S. 1978, *ApJ*, 220, 643
- Schmitt, D., & Degenhardt, U. 1995, *Rev. Mod. Astron.*, 8, 61
- Schutgens, N. A. J. 1997a, *A&A*, 323, 969
- . 1997b, *A&A*, 325, 352
- Schutgens, N. A. J., & Tóth, G. 1999, *A&A*, 345, 1038
- Soler, R., Oliver, R., & Ballester, J. L. 2007a, *A&A*, 471, 1023 (Paper I)
- . 2007b, *Sol. Phys.*, 246, 73
- . 2008, *NewA*, submitted
- Spruit, H. C. 1982, *Sol. Phys.*, 75, 3
- Terradas, J., Carbonell, M., Oliver, R., & Ballester, J. L. 2005, *A&A*, 434, 741
- Terradas, J., Molowny-Horas, R., Wiehr, E., Balthasar, H., Oliver, R., & Ballester, J. L. 2002, *A&A*, 393, 637
- Terra-Homem, M., Erdélyi, R., & Ballai, I. 2003, *Sol. Phys.*, 217, 199
- Tsubaki, T., & Takeuchi, A. 1986, *Sol. Phys.*, 104, 313
- van der Linden, R. A. M., & Goossens, M. 1991, *Sol. Phys.*, 131, 79
- Yi, Z., & Engvold, O. 1991, *Sol. Phys.*, 134, 275
- Yi, Z., Engvold, O., & Kiel, S. L. 1991, *Sol. Phys.*, 132, 63
- Zirker, J. B., Engvold, O., & Martin, S. F. 1998, *Nature*, 396, 440